Accepted Version
Published version available in Materials Letters *at* 10.1016/j.matlet.2021.131212

Electrospun V_2O_5 Nanofibers as High-Capacity Cathode Materials for Zinc-Ion Batteries

A. I. Volkov [a]*, A. S. Sharlaev [b], O. Ya. Berezina [b], E. G. Tolstopjatova [a], L. Fu [c], V. V. Kondratiev [a]

[a] Saint Petersburg State University, 7/9 Universitetskaya nab., St. Petersburg, 199034, Russian Federation

[b] Institute of Physics and Technology, Petrozavodsk State University, Petrozavodsk, 185910, Russian Federation

[c] State Key Laboratory of Materials-Oriented Chemical Engineering, College of Energy Science and Engineering, and College of Chemical Engineering, Nanjing Tech University, Nanjing 211816, Jiangsu Province, China

*email: grulfex@gmail.com

Abstract

Vanadium pentoxide (V_2O_5) has attracted significant attention in recent years as a cathode material for aqueous zinc-ion batteries (AZIBs). Its unique layered structure allows for reversible intercalation of various multivalent ions, including Zn^{2+}.

This paper proposes a sol-gel electrospinning method for preparation of vanadium pentoxide nanofibers, followed by thermal treatment in air. The composition and structure of the obtained powders were verified by X-ray diffraction, energy-dispersive X-ray elemental analysis, and X-ray photoelectron spectroscopy, while the morphology of the samples was investigated by scanning electron microscopy. The electrochemical properties and performance of the electrode materials based on V_2O_5 nanofibers were studied using cyclic voltammetry, galvanostatic charge-discharge, and electrochemical impedance spectroscopy methods. V_2O_5 electrodes demonstrate high specific capacity (357 mA h g^{-1} at 0.05 A g^{-1}) and good long-term cyclic stability.

Keywords: aqueous zinc-ion batteries, electrospinning, vanadium pentoxide, electrode materials

1. Introduction

Aqueous zinc-ion batteries (AZIBs) are a major area of interest within the field of multivalent rechargeable batteries [1]. Among other candidates for the next-generation power sources, AZIBs are promising due to their high safety, cost effectiveness and environmental friendliness [1,2].

Vanadium pentoxide has gained attention as a cathode material with capability for reversible intercalation of Zn^{2+} ions and high (295 mA h g^{-1}) theoretical capacity [2]. However, research has consistently shown that V_2O_5 cathodes lack conductivity, and phase transitions of layered structures upon Zn^{2+} intercalation cause capacity fading [2–5]. Preliminary inclusion of Zn into the structure alleviates some of these issues, simultaneously showing reversibility of Zn^{2+} intercalation in such structures [6,7]. In addition to that, H^+ intercalation in such materials also occurs, which has been both observed experimentally [5,8] and confirmed computationally [9].

Existing research recognizes the critical role played by nanostructuring of active material in electrodes activation process, their capacity, and stability. This strategy is one of the effective ways to enhance the electrochemical performance of V_2O_5 cathodes in AZIBs [4,10,11]. The increase of specific capacity values in such cases is due to surface processes in addition to intercalation. As the material activates during initial cycles, Zn^{2+} intercalation contribution increases, facilitated by water molecules insertion into the material structure. As a result, stable vanadium oxide-based electrode materials with capacities as high as (315–430) mA h g^{-1} have been reported [4,7,8,11].

This paper proposes the use of electrospun V_2O_5 nanofibers as an active material in cathodes for AZIBs. We show that this simple and effective method, suitable for large-scale production of V_2O_5 nanofibers, allows to obtain high-capacity electrodes with prospective functional properties for application in AZIBs.

2. Materials and methods

The V_2O_5 nanofiber samples were synthesized by electrospinning from the solution, prepared by dissolving vanadium oxide precursors in hydrogen peroxide, followed by dissolving binding polymer polyvinylpyrrolidone (PVP) (M_r = 1.3·10^6 g mol^{-1}). The synthesis was performed through a 0.7 mm needle at the flow rate of 0.5 ml h^{-1} at the applied potential difference of (15–18) kV. Then, the nanofibers were annealed in air at 500 °C for 1 h, with the 5 °C min^{-1} heating and cooling rates to remove the PVP and crystallize the oxide fibers.

Electrode materials were prepared by mixing V_2O_5 nanofibers (70 wt.%), carbon black (20 wt.%) and polyvinylidene fluoride (10 wt.%) in N-methylpyrrolidone. The resulting viscous slurry was cast on the titanium foil, dried at 80 °C in vacuum overnight, and pressed, then the electrodes (0.88±0.07 mg of

active material) were punched. CR2032 coin cells were assembled with Zn foil as anode with 3.5 mol dm^{-3} $ZnSO_4$ as electrolyte and glass fiber membranes soaked in the electrolyte as separators. The V_2O_5 electrodes were studied by cyclic voltammetry (CV), galvanostatic charge-discharge (GCD) in a (0.3—1.5) V (vs. Zn/Zn^{2+}) potential range, and electrochemical impedance spectroscopy (EIS) using Autolab PGSTAT30, Bio-Logic VMP-3 and Neware BTS4000.

The structure and morphology of the materials were studied by high-resolution X-ray diffraction (Cu Kα, Bruker-AXS D8 DISCOVER), energy dispersive X-ray spectroscopy, scanning electron microscopy (SUPRA 40VP Carl Zeiss), optical microscopy, and X-ray photoelectron spectroscopy (Thermo Fisher Scientific Escalab 250Xi).

3. Results and discussion

As-prepared nanofibers contain PVP and thus have a higher diameter than annealed ones (Figure S1). The samples (Figure 1a,b) have a tubular non-smooth surface. The fibers of the material consist of granules connected into strands with an average diameter of (390±10) nm (Figure 1e).

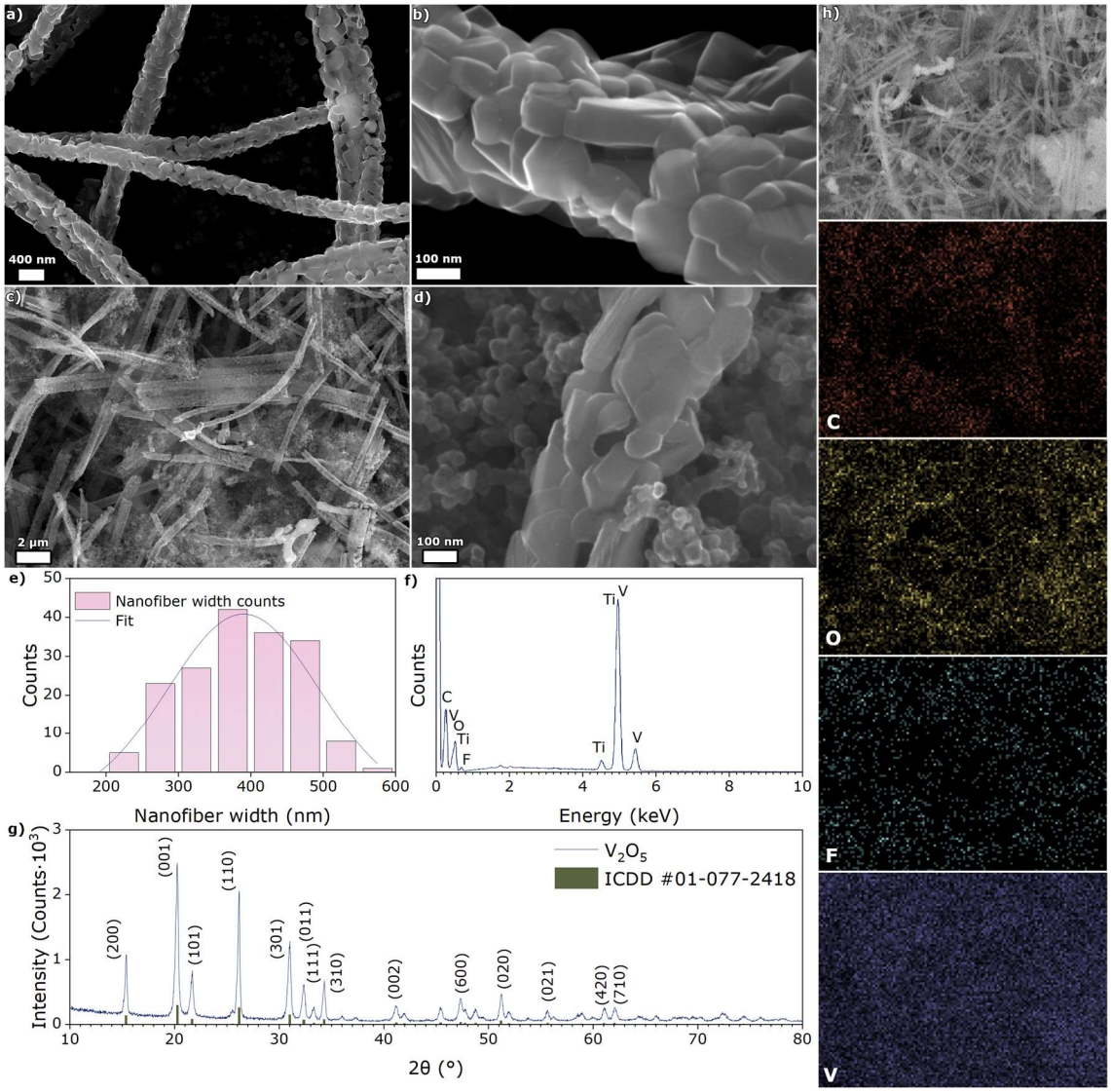

Figure 1. SEM images of annealed V_2O_5-nanofibers (a,b) and V_2O_5-based electrode material (c,d); distribution of nanofibers diameter (e), EDX spectrum of the electrode material (f), XRD spectrum of V_2O_5 nanofibers (g), and elemental mapping for electrode material (h).

In the fabricated electrode material (Figure 1c,d), the distribution of particles contains free volume and large surface are for electrolyte access. The EDX elemental mapping (Figure 1h) shows the complete coating of the substrate with vanadium-containing species, and a typical spectrum (Figure 1f) provides a 1.8:1 oxygen to vanadium ratio.

XRD spectrum of the sample (Figure 1g) corresponds to orthorhombic V_2O_5 (ICDD card no. 07-077-2418, *Pmmn* (59) space group). Interlayer distance for (001) plane is 4.4 Å, which is close to previously reported values [3]. Additional characterization of the material includes O 1s and V 2p XPS

spectra (Figure S2), that show that vanadium is present in V^{5+} and V^{4+}, which is consistent with the literature [3,12].

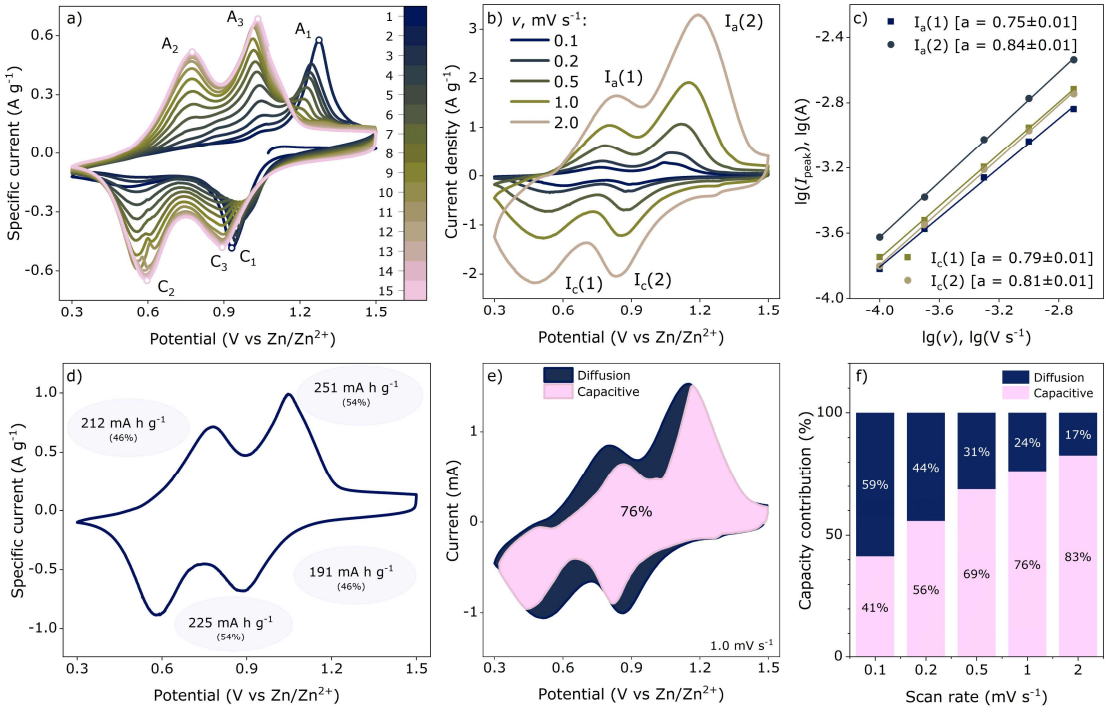

Figure 2. a) CVs of V_2O_5 nanofiber electrodes at 0.2 mV s^{-1} during initial 15 cycles, b) CVs at different scan rates, c) linear fit of peak currents vs scan rate and estimated a *coefficient for V_2O_5 nanofiber electrodes, d) stable CV at 0.2 mV s^{-1} with contribution of separate redox peaks to total capacity, e) capacitive and diffusion contributions at 1 mV s^{-1}, f) capacitive contribution at different scan rates.*

The shape of CVs (Figure 2a) recorded in the 0.3 V to 1.5 V range transforms during initial cycles as V_2O_5 structure changes. At 0.2 mV s^{-1} this usually takes up to 20 cycles. At first, a pair of peaks at 1.28 V (A_1) and 0.95 V (C_1) prevails. After the transformation, two pairs of stable peaks appear at 0.78 V (A_2) / 0.58 V (C_2), and 1.05 V (A_3) / 0.88 V (C_3), which probably correspond to the consecutive redox process of V^{5+} to V^{3+}, with V^{4+} as an intermediate state [10], forming $Zn_xV_2O_5$ phases with different degrees of Zn^{2+} intercalation (ex situ XRD in Figure S3) [13]. Alternatively, both Zn^{2+} and protons intercalation may occur, as per recent studies [5,9]. Upon reaching stability, a CV contains two pairs of peaks, and each peak contributes equally to the total capacity (Figure 2d). This indicates that intercalation of Zn^{2+} ions is accompanied by phase transitions with formation of new structures with stable reversible charge-discharge processes.

The separation of peaks upon scan rate increase (Figure 2b) allows to evaluate electrochemical kinetics by fitting the peak currents vs scan rate dependence (Figure 2c). The obtained *b* values from 0.75 to 0.84 indicate that all occurring processes are of mixed nature, combining both interfacial Zn^{2+} storage ($b \rightarrow 1.0$) and diffusion-controlled redox reaction ($b \rightarrow 0.5$).

Capacitive and diffusion current contributions were differentiated via the method proposed by Dunn [14]. At a higher scan rate, i.e., at 1.0 mV s^{-1} (Figure 2e), 76% of total currents is due to capacitive effects, which agrees with high availability of the surface area. At various scan rates (Figure 2f), the capacitive contribution reaches 81%, while at lower scan rates diffusion-controlled currents prevail with 59% of total capacity value.

Like CVs, GCD curves show the evolution of the recharging processes in the initial cycles. The specific capacity of the V_2O_5 cathode increases (Figure 3a) up to ~350 mA h g^{-1}, where it levels. Increased surface availability of V_2O_5 particles, as seen from SEM images and confirmed by substantial capacitive currents contribution in CVs, is the reason of high specific capacity values. Additionally, reorganization of the material crystal lattice [8,12] causes such increase from 176 mA h g^{-1} in the 2nd cycle. Within these cycles, an oxidation plateau shifts from an average potential of 1.17 V to 1.04 V. Meanwhile, the reduction plateau only shifts slightly from 1.00 V to 0.97 V. This reduces the ΔE between anodic and cathodic plateaus, indicating facilitation of redox processes. Simultaneously, the capacity of the oxidation process in the plateau with a 0.72 V average potential increases, with its reduction counterpart at 0.65 V.

The material shows decent rate capability (Figure 3b,c): the initial capacity is 282 mA h g^{-1} at 0.1 A g^{-1}, of which 179 mA h g^{-1} (or 63%) remain at 2 A g^{-1}. At higher current densities, no significant changes of plateaus potentials occur, though iR-drop increases, and the slope of the curves indicates a slightly more capacitor-like response, consistently with CV analysis. The behavior of cycle life trend (Figure 3d) at fixed 0.1 A g^{-1} current density after initial "activation" of the material at 0.05 A g^{-1} shows the presence of maximum capacity within the first few cycles. For more continuous studies, we applied 2 A g^{-1} (Figure 3e), where the capacity maximum is also present, consistently with published research [3,5,15]. The specific capacity in the second cycle is 74 mA h g^{-1}, which increases to 211 mA h g^{-1} by the 27th cycle, from where a steady decline starts. Gradual expansion of the interlayer distance due to Zn^{2+} intercalation and formation of $Zn_xV_2O_5$ phase may cause such "activation" process, simultaneously

tipping the ratio of Zn^{2+} and H^{+} intercalation in favor of Zn^{2+} [6,8]. By the 500th cycle, capacity is 101% of the initial value, yet only 36% of maximum value. This may be because of trapped Zn^{2+} ions decreasing material availability [15]. The speed of such transformation is dependent on the mode of electrochemical impact on the system: it takes nearly 30 GCD cycles at 0.2 A g^{-1} to achieve maximum performance, while CV at 0.2 mV s^{-1} does that in 15 cycles. This warrants further investigations of the recharging mechanism, yet its complete study is well beyond the scope of this paper.

The transformation of the material, and the related increase of specific capacity affect the EIS (Figure 3f). The equivalent circuit is a slight modification of reported ones [4,11]. The contributing resistance values are less in the "activated" material: 27 Ω and 85 Ω for charge transfer resistances R_1 and R_2 versus initial 91 Ω and 124 Ω, respectively (see fitted values in Table S1). This allows for the increase of capacity because of the facilitation of charge transfer. Such results are in line with the morphology studies that show high-surface samples, and significant capacitive currents contribution in CV studies additionally confirm that.

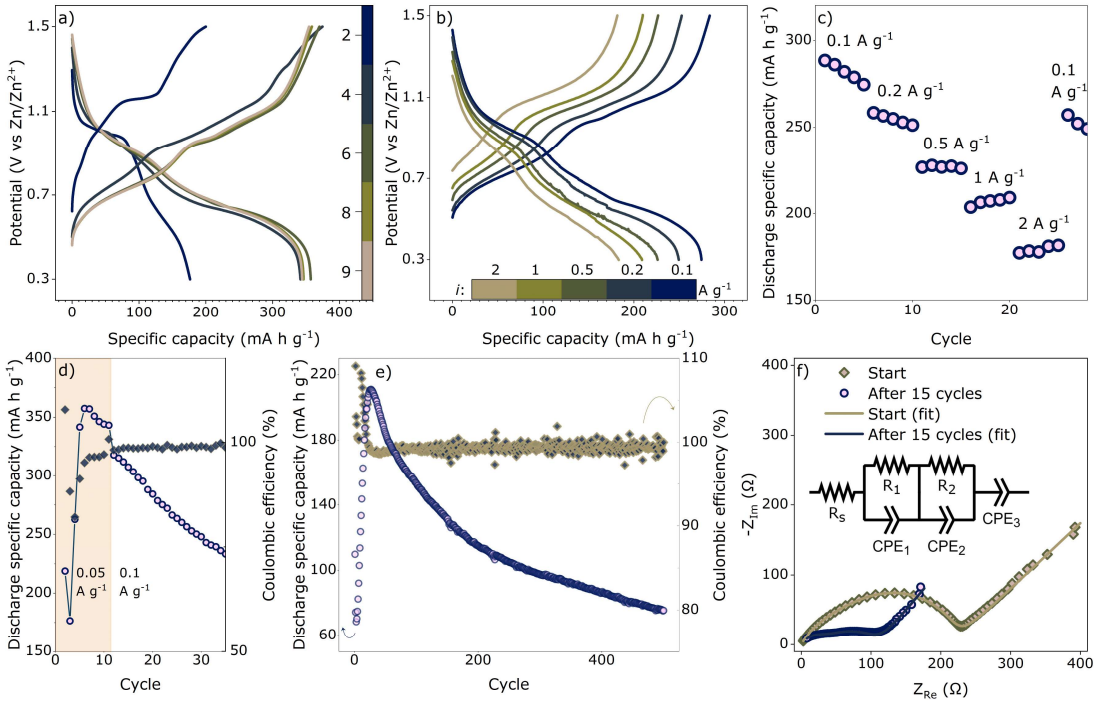

Figure 3. Selected GCD curves within the initial 10 cycles at 0.05 A g^{-1} (a), and at different current densities (b); current density capability (c), cyclic stability at 0.05 A g^{-1} and 0.1 A g^{-1} (d) and 0.2 A g^{-1} (e), EIS in the beginning and after 15 cycles for V_2O_5 electrodes (f).

4. Conclusions

A facile electrospinning method of V_2O_5 nanofibers synthesis allows to obtain the cathode materials for rechargeable AZIBs with high specific capacities of up to 282 mA h g^{-1} and enhanced C-rate capability at currents from 0.1 A g^{-1} to 2.0 A g^{-1}. EIS confirms facilitation of charge transfer after material activation by multiple recharging cycles. The electrodes retain remarkable electrochemical activity after 500 cycles. A rather simple and effective electrospinning method is shown to be promising for large-scale production of V_2O_5 nanofibers allowing to obtain prospective high-capacity electrodes for application in AZIBs.

Acknowledgements

The financial support from RFBR (project № 21-53-53012) and National Natural Science Foundation Committee of China (project № 51772147, 52111530050) is gratefully acknowledged. The authors would like to thank the Centre for X-ray Diffraction Studies, Centre for Physical Methods of Surface Investigation, and the Interdisciplinary Resource Centre for Nanotechnology of Research Park of Saint Petersburg State University.

References

[1] X. Zhao, X. Liang, Y. Li, Q. Chen, M. Chen, Challenges and design strategies for high performance aqueous zinc ion batteries, Energy Storage Mater. 42 (2021) 533–569. doi:10.1016/j.ensm.2021.07.044.

[2] V. Mathew, B. Sambandam, S. Kim, S. Kim, S. Park, S. Lee, M.H. Alfaruqi, V. Soundharrajan, S. Islam, D.Y. Putro, J.Y. Hwang, Y.K. Sun, J. Kim, Manganese and Vanadium Oxide Cathodes for Aqueous Rechargeable Zinc-Ion Batteries: A Focused View on Performance, Mechanism, and Developments, ACS Energy Lett. 5 (2020) 2376–2400. doi:10.1021/acsenergylett.0c00740.

[3] D. Chen, X. Rui, Q. Zhang, H. Geng, L. Gan, W. Zhang, C. Li, S. Huang, Y. Yu, Persistent zinc-ion storage in mass-produced V_2O_5 architectures, Nano Energy. 60 (2019) 171–178. doi:10.1016/j.nanoen.2019.03.034.

[4] F. Yang, Y. Zhu, Y. Xia, S. Xiang, S. Han, C. Cai, Q. Wang, Y. Wang, M. Gu, Fast Zn^{2+} kinetics of vanadium oxide nanotubes in high-performance rechargeable zinc-ion batteries, J. Power Sources. 451 (2020) 227767. doi:10.1016/j.jpowsour.2020.227767.

[5] W. Liu, L. Dong, B. Jiang, Y. Huang, X. Wang, C. Xu, Z. Kang, J. Mou, F. Kang, Layered vanadium oxides with proton and zinc ion insertion for zinc ion batteries, Electrochim. Acta. 320 (2019) 134565. doi:10.1016/j.electacta.2019.134565.

[6] L. Wang, K.W. Huang, J. Chen, J. Zheng, Ultralong cycle stability of aqueous zinc-ion batteries with zinc vanadium oxide cathodes, Sci. Adv. 5 (2019) 1–11. doi:10.1126/sciadv.aax4279.

[7] P. Luo, W. Zhang, S. Wang, G. Liu, Y. Xiao, C. Zuo, W. Tang, X. Fu, S. Dong, Electroactivation-induced hydrated zinc vanadate as cathode for high-performance aqueous zinc-ion batteries, J. Alloys Compd. 884 (2021) 161147. doi:10.1016/j.jallcom.2021.161147.

[8] R. Li, H. Zhang, Q. Zheng, X. Li, Porous V_2O_5 yolk-shell microspheres for zinc ion battery cathodes: Activation responsible for enhanced capacity and rate performance, J. Mater. Chem. A. 8 (2020) 5186–5193. doi:10.1039/c9ta11750d.

[9] X. Liu, H. Euchner, M. Zarrabeitia, X. Gao, G.A. Elia, A. Groß, S. Passerini, Operando pH measurements decipher H^+/Zn^{2+} intercalation chemistry in high-performance aqueous Zn/δ-V_2O_5 batteries, ACS Energy Lett. 5 (2020) 2979–2986. doi:10.1021/acsenergylett.0c01767.

[10] B. Sambandam, V. Soundharrajan, S. Kim, M.H. Alfaruqi, J. Jo, S. Kim, V. Mathew, Y.K. Sun, J. Kim, Aqueous rechargeable Zn-ion batteries: An imperishable and high-energy $Zn_2V_2O_7$ nanowire cathode through intercalation regulation, J. Mater. Chem. A. 6 (2018) 3850–3856. doi:10.1039/c7ta11237h.

[11] Y. Li, P. Xu, J. Jiang, J. Yao, B. Huang, J. Yang, Facile synthesis of ultra-large V_2O_5 xerogel flakes and its application as a cathode material for aqueous Zn-ion batteries, Mater. Today Commun. 26 (2021) 101849. doi:10.1016/j.mtcomm.2020.101849.

[12] Y. Lu, T. Zhu, W. van den Bergh, M. Stefik, K. Huang, A High Performing Zn-Ion Battery Cathode Enabled by In Situ Transformation of V_2O_5 Atomic Layers, Angew. Chemie - Int. Ed. 59 (2020) 17004–17011. doi:10.1002/anie.202006171.

[13] M. Yan, P. He, Y. Chen, S. Wang, Q. Wei, K. Zhao, X. Xu, Q. An, Y. Shuang, Y. Shao, K.T. Mueller, L. Mai, J. Liu, J. Yang, Water-Lubricated Intercalation in $V_2O_5{\cdot}nH_2O$ for High-Capacity and High-Rate Aqueous Rechargeable Zinc Batteries, Adv. Mater. 30 (2018) 1–6. doi:10.1002/adma.201703725.

[14] J. Wang, J. Polleux, J. Lim, B. Dunn, Pseudocapacitive contributions to electrochemical energy storage in TiO_2 (anatase) nanoparticles, J. Phys. Chem. C. 111 (2007) 14925–14931. doi:10.1021/jp074464w.

[15] S. Wu, Y. Ding, L. Hu, X. Zhang, Y. Huang, S. Chen, Amorphous V_2O_5 as high performance cathode for aqueous zinc ion battery, Mater. Lett. 277 (2020) 128268. doi:10.1016/j.matlet.2020.128268.